Trans Indian Inst Met (2021) 74(6):1295–1301
https://doi.org/10.1007/s12666-021-02224-7

ORIGINAL ARTICLE

Effects of Primary Stored Energy on Relaxation Behavior of High Entropy Bulk Metallic Glasses Under Compressive Elastostatic Loading

Israa Meften Hashim[1] · Israa Faisal Ghazi[2] · Oleg R. Kuzichkin[3] · Indira A. Shakirova[4] · A. Surendar[5] · Lakshmi Thangavelu[5] · Aleksei Evgenievich Dorofeev[6] · Yu Zhu[7]

Received: 8 October 2020 / Accepted: 18 February 2021 / Published online: 14 March 2021

Abstract This paper aims to show the effects of primary stored energy in high entropy bulk metallic glasses (HE-BMGs) on their relaxation behavior after elastostatic loading process. For this purpose, three HE-BMGs with different chemical compositions and primary stored energy were fabricated. Differential scanning calorimetry and nanoindentation tests were carried out to evaluate the relaxation enthalpy and microscopic mechanical characterization of alloys. The results showed that increase in the number of element types in the alloying composition leads to the increment of stored energy and structural heterogeneity in the primary alloys. Moreover, the elastostatic loading rejuvenates the primary alloys; however, an optimum heterogeneity is needed for the maximum structural heterogeneity and stored energy in the glassy alloy. The hardness measurements also indicate that the elastostatic loading intensifies the hardness variations in the alloys, which may be due to the increased structural heterogeneity.

Keywords High entropy metallic glass · Relaxation · Stored energy · Rejuvenation

✉ A. Surendar
Surendararavindhan@ieee.org

✉ Yu Zhu
yuzhu6494@gmail.com

1 Nursing College/University of Al_Qadisiyah, Al Diwaniyah, Iraq

2 Department of Materials Engineering, Engineering College, University of Al-Qadisiyah, Al Diwaniyah, Iraq

3 Department of Information and Robototechnic Systems, Belgorod State University, Belgorod, Russia 308015

4 Kazan Federal University, Kazan, Russia

5 Department of Pharmacology, Saveetha Dental College and Hospital, Saveetha Institute of Medical and Technical Sciences, Chennai, India

6 Department of Propaedeutics of Dental Diseases, Sechenov First Moscow State Medical University, Moscow, Russia

7 School of Mechanical Engineering, Jiangsu University, Zhenjiang 212013, Jiangsu, China

1 Introduction

Due to their unique structural characteristics at angstrom-scale arrangements, metallic glasses (MGs) show outstanding physical behavior and excellent mechanical properties [1–4]. On the other side, recently another classification of metallic materials has been developed, namely high entropy alloys, with several equally elemental constitutes and single solid solution phase leading to a broad range of individual properties [5–9]. In recent years, the experimental results have shown that the strategy for development and fabrication of the high entropy, when employed with care, works efficiently in the design of new BMG materials with excellent properties such as better glass forming ability (GFA) and higher mechanical behaviors compared to the conventional BMGs [10]. Merging inherent traits of BMG and high entropy systems, researchers have recently shown that it is possible to design and produce high entropy alloys with one monolithic amorphous structure [11–13]. This combination of materials characteristics has led to the production of novel materials, i.e., high entropy BMG (HE-BMG), with promising functional and mechanical properties [14–17]. For instance, Wang et al. [18] showed that the thermoplastic formability of TiZrHfNiCuBe alloy strongly depends on Newtonian flow and it can be improved by vibrational loading. Yin et al. [19] proposed a cryogenic

method evaluation facilitating the analysis of low temperature magnetocaloric effect of high entropy metallic glasses. In another work, Huo et al. [20] developed a denary alloy possessing large magnetic entropy variations over a broad range of temperature and has a large refrigerant capacity. In another work, $Fe_{26.7}Co_{26.7}Ni_{26.6}Si_9B_{11}$ HE-BMG was fabricated and the corresponding studies indicated that the alloy proposes a good bending ductility and superior soft magnetic properties [21]. Wang et al. [22] reported that the HE-BMGs are also capable to tolerate the harmful ion irradiation effects and exhibit a favorable response to high levels of helium implantation. Tong et al. [23] investigated the effects of aspect ratio on serrated flow dynamic and plasticity of TiZrHfCuNiBe HE-BMG and found that the plasticity and serration size are not monotonic correlated. The tensile creep evaluation of $Al_{20}Ce_{20}La_{20}Ni_{20}Y_{20}$ HE-BMG also reveals that the extension and retardation of smaller defects in the structure lead to the significant increase in activation energy of tensile creep [24]. Gu et al. [25] correlated the structural heterogeneity in HE-BMG to the stored energy level and reported that the cryogenic treatment extraordinarily improves the stored energy in the structure. Duan et al. [26] linked the shear modulus to the enthalpy variations of high entropy alloy and found that the thermal flow and shear softening rely on anharmonicity of interatomic potential.

As described, the HE-BMG alloys are promising materials for various applications with different physical and mechanical features. However, the perception of their structural characteristics and relaxation behavior is a common challenge for any application. In this work, we have developed new HE-BMG compositions with different primary stored energy and performed a subsequent elastostatic treatment to show that how the structural heterogeneity, which links to the primary stored energy, induces the energy intensification in the material.

2 Experimental Procedure

Three alloys with nominal compositions of $Ti_{20}Zr_{20}Be_{20}Hf_{20}Cu_{20}$, $Ti_{20}Zr_{20}Be_{20}Hf_{20}Cu_{10}Ni_{10}$ and $Ti_{20}Zr_{20}Be_{20}Hf_{20}Cu_{10}Ni_5Y_5$ were cast by arc-melting technique under Ti-gettered argon environment. The prepared alloys were then fabricated in the form of 2 mm-diameter rods using copper mold casting method. The primary samples, i.e., $Ti_{20}Zr_{20}Be_{20}Hf_{20}Cu_{20}$, $Ti_{20}Zr_{20}Be_{20}Hf_{20}Cu_{10}Ni_{10}$ and $Ti_{20}Zr_{20}Be_{20}Hf_{20}Cu_{10}Ni_5Y_5$, were coded as S1, S2 and S3 in the paper, respectively. X-ray diffraction (XRD) analysis was performed to ensure the amorphousness of prepared alloys. Elastostatic loading, as a rejuvenation treatment [27, 28], was then carried out to affect the stored energy in the amorphous alloys. The treatment was done for 24 h at room temperature under 98% yield strength of the alloys. Similar to their codes for their primary situations, the rejuvenated samples were coded as S11, S22 and S33, respectively. For elastostatic loading process, the samples were cut from the reference rods with the length of 4 mm. The sample cross sections were carefully polished to avoid any experimental error. After the treatment, differential scanning calorimeter (DSC) test with heating rate of 20 K/min under argon atmosphere was employed to evaluate the relaxation enthalpy changes in the HE-BMGs. For each sample, we did DSC experiment three times to ensure the reproducibility. Moreover, nanoindentation experiment was considered for studying micromechanical characteristics and structural heterogeneity. The experiment was done with samples taken from the cross sections at the center region. The maximum load was 15 mN and the load rate was set as 0.5 mN/s. To obtain cumulative curves, the 90 indentation points were considered. To evaluate the anelasticity, high-rate nanoindentation test was done with holding time, loading time and unloading time of 0.05 S, 0.005 S and 0.05 S, respectively. Using Mitutoyo HM tester, microhardness measurements were also carried out at the cross section from the center to the edges with 10 S load time and load of 40 gr.

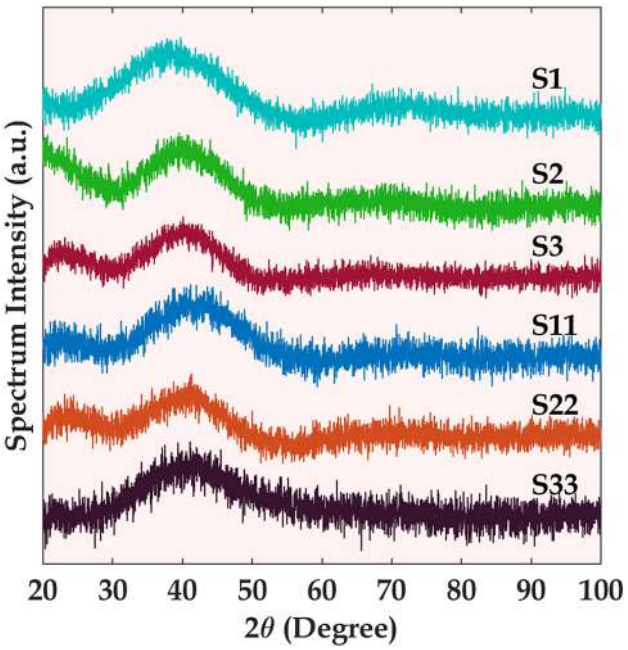

Fig. 1 XRD patterns of as-cast and rejuvenated samples

3 Results and Discussion

At the first step, it is important to affirm the amorphousness of HE-BMG samples. According to the XRD results (Fig. 1), there are no sharp peaks in the patterns, which confirm the lack of crystalline phases in the microstructure. Figure 2a illustrates the relaxation region of HE-BMG samples located under the glass transition temperature (T_g). The exothermic heat release in the relaxation region defines the value of stored energy in the amorphous structure. The results show that the elastostatic loading leads to the increase in the stored energy of all the samples. The increment in stored energy is related to the excitation of atomic configurations and intensification of disordered structures in the amorphous material [29, 30]. Figure 2b presents the relaxation enthalpy values, as indicator of stored energy, for all the samples. As observed, the primary stored energy in the HE-BMG alloys strongly depends on the chemical composition so that with the addition of more element types into the alloy composition, the primary stored energy significantly increases. Accordingly, it is derived that the increase in the number of element types in the alloying compositions leads to the improvement of elemental heterogeneity in the material and consequently, intensifies the nano-scale defects such as free volumes in the atomic structure. The measured relaxation enthalpy for S1, S2 and S3 is 4.9, 5.7 and 6.1 J/g, respectively, which indicates the elemental heterogeneity effects on the primary stored energy. On the other side, the elastostatic loaded samples show a different trend so that the measured relaxation enthalpy for S11, S22 and S33 is 5.5, 7.1 and 6.7 J/g, respectively. This result indicates that primary elemental heterogeneity markedly influences the subsequent relaxation enthalpy increment, achieved from the elastostatic loading. In fact, an optimum heterogeneity is needed for the maximum stored energy in the atomic structure.

To evaluate the microscopic mechanical properties, the cast samples along with their rejuvenated states were tested by nanoindentation technique. Using Oliver and Pharr method, the nanohardness trend was also extracted from the unloading curves. According to load–displacement curves given in Fig. 3a, the intensification of curves slope relies on the chemical composition and the subsequent stored energy during the elastostatic loading. The maximum detected displacement for sample S22 indicates that the rejuvenation process is potentially optimum for the primary samples and correlates to the primary stored energy in the material. As observed in Fig. 3b, c, the improvement in plasticity is accompanied with the decrease in the young modulus and hardness. In other words, the enhanced ductility under elastostatic loading comes at the expense of hardness of material. Figure 3 apparently indicates the effects of elastostatic loading on the microscopic mechanical properties of samples. One can see that the measured features have linear trends for the primary samples, while the feature variations for elastostatic loaded samples show a peak/valley trend. This result

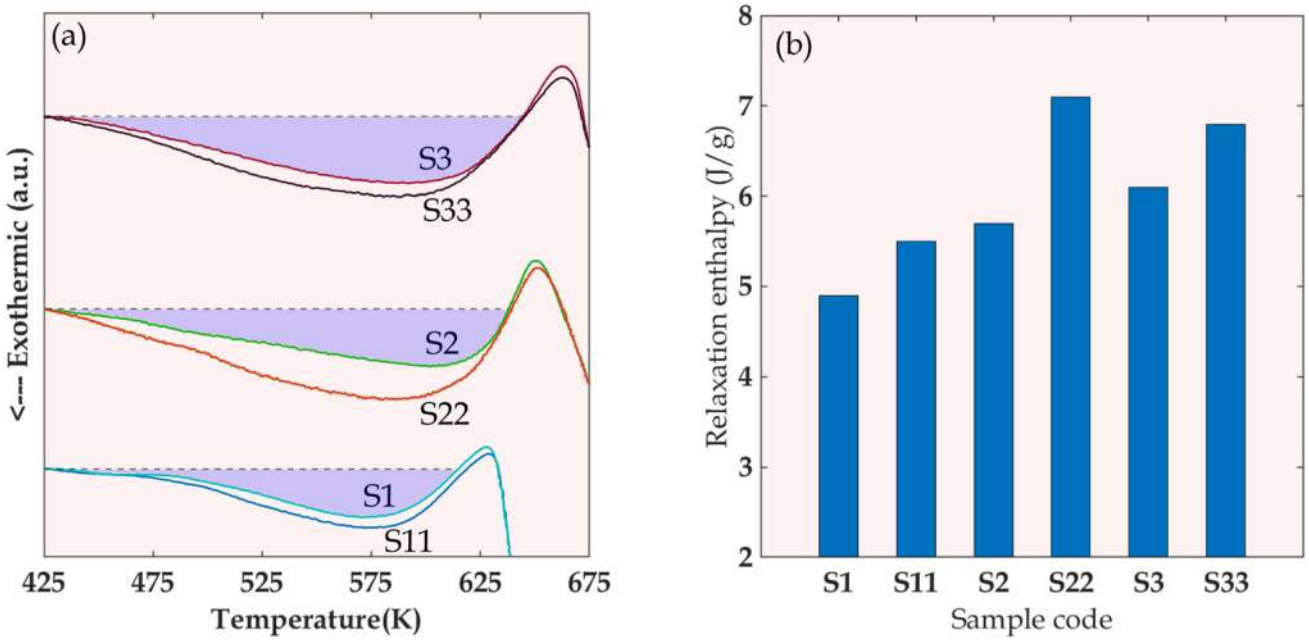

Fig. 2 **a** Relaxation enthalpy region in DSC curves of samples, **b** relaxation enthalpy values for the samples

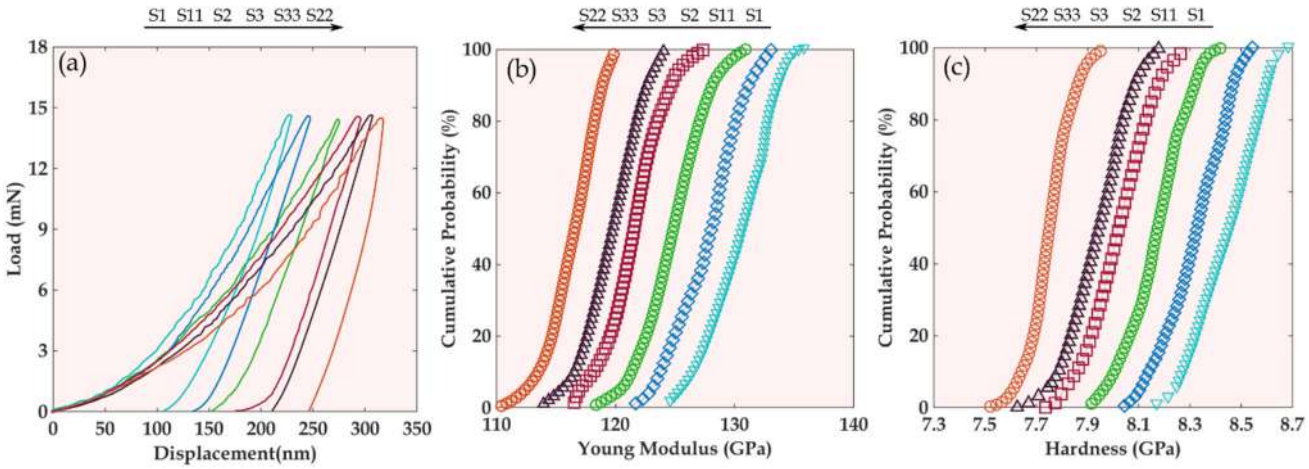

Fig. 3 **a** Load–displacement curves of samples in nanoindentation test, and cumulative distribution of **b** Young's modulus, **c** hardness

confirms that the primary chemical heterogeneity, which is related to the number of element types, plays the most important role in the rejuvenation. To better understand the role of heterogeneity, the nanoindentation test with high strain rate was performed. As reported in previous works, the nanoscale compositional changes along with the local density variations are indicators of structural heterogeneity in the BMG alloys [31, 32]. In other words, the heterogeneous elemental distribution in the amorphous structure is related to the random formation of dense packing regions, namely short and medium range orders, and embedded loose packing regions such as free volumes [33, 34]. Considering this explanation, when an external dynamic force is applied on the sample, the high density structures respond in an elastic manner, while the loose packing regions experience an anelastic deformation. Under the high-rate indenting process, the hysteresis loop of loading and unloading curve introduces the range of anelasticity in the material. The following equation correlates the nanoindentation curve to the viscoelastic model [25]:

$$h(t)^{3/2} = \frac{3 \cdot p(t) \cdot (1-v)}{8G_1 R^{1/2}} - \frac{3P'(1-v)G_2 \cdot t_c}{8G_1 R^{\frac{1}{2}} \cdot (G_1+G_2)} \left[1 - \exp\left(-\frac{t}{t_c}\right)\right] \quad (1)$$

In which R and v are the tip radius and poisson's ratio, respectively. P' is the loading rate, t_c defines the relaxation time and, G_1 and G_2 introduce the modulus of dense- and loose-packing structures, respectively. Fitting the mentioned equation and the load–displacement curve, it is possible to attain G_1 and G_2 data and subsequently, the volume fraction of loose packing structures can be achieved as follows [35]:

$$\text{loosepackingfraction}\% = \frac{G_2}{(G_1+G_2)} \quad (2)$$

According to Fig. 4, the fraction volume of loose packing structures for S1, S2 and S3 is 9.9%, 12.9% and 13.4%, respectively. Previous works showed that the fraction volume of loose structure for conventional metallic glasses is in the range of 20–25%, which is much higher than our results [35, 36]. It is suggested that when an element is dominant in the atomic structure and several minor added elements are in the chemical compositions, the disordering phenomenon can be intensified in the microstructure. This means that variety of short range order clusters with different symmetries and sizes increases, and therefore the nanoscale defects, i.e., loose structures get enhanced in the material. On the other side, HE-BMGs have several elements with equal contents leading to the formation of short range scale clusters with close symmetries and sizes. As a result, the atomic structure tends to form a backbone with a low possible defects. As observed, when the minor addition increases in the chemical compositions from S1 to S3, the glassy material induces more loose packing structures. Another point should be noted is the trend of loose structure fraction after the elastostatic loading. According to the results, an optimum loose structure in the primary structure of sample is needed to obtain the maximum stored energy or uppermost heterogeneity after elastostatic loading. When the structure is more homogeneous (S1), the short and medium range orders are dominant and the defects are isolated. Under this condition, the glassy alloy has strong bonds and consequently, the force during the elastostatic loading is not enough to break down the ordered structure and induce more heterogeneity. Hence, one can see that the stored energy or loose-structure fraction show a minor

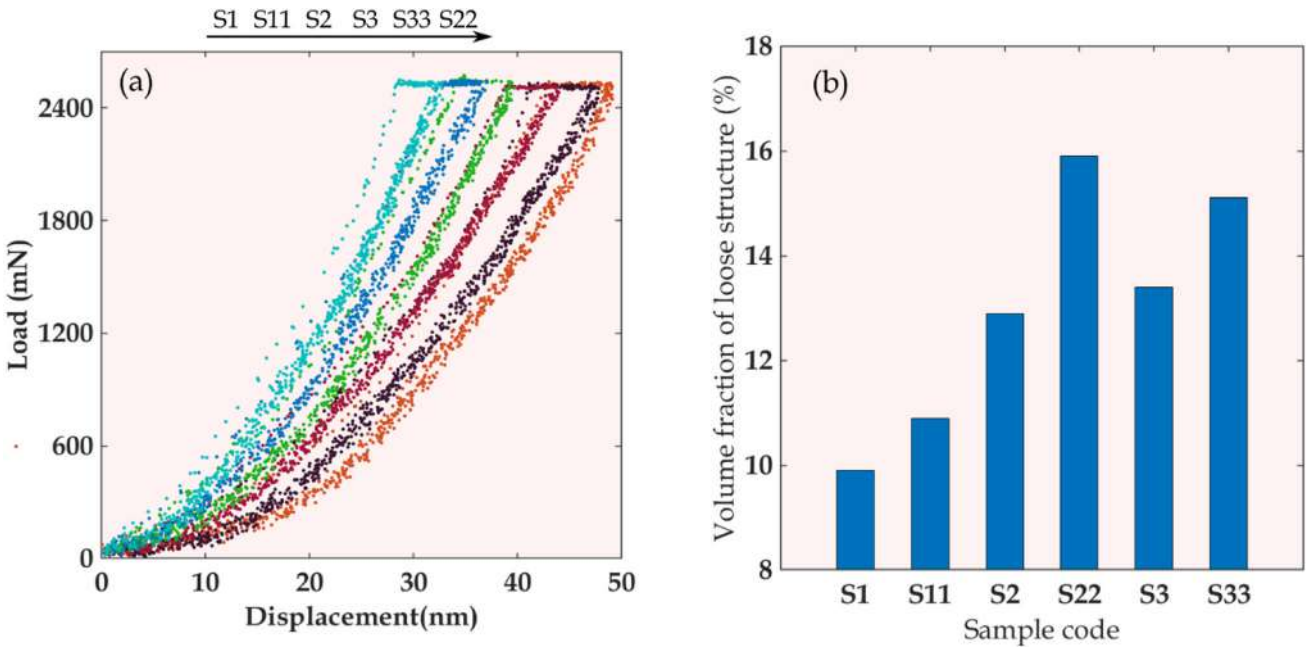

Fig. 4 **a** Load–displacement curves of samples under high-rate nanoindentation test, **b** volume fraction of loose packing structures

increase in sample S11. On the other side, the sample S3 with the highest primary heterogeneity is not able to produce the highest stored energy or loose-structure fraction (S33). It is believed that the high primary structural heterogeneity in S3 has excessive defects, i.e., free volume, in the glassy configuration. Hence, when the elastostatic loading is applied to this sample, the excessive weak bonds in free volume regions relax the stress domains and prevent the formation of new defects in the microstructure. With all these descriptions, sample S2 with optimum primary stored energy induces more structural heterogeneity and nanoscale defects after elastostatic loading (S22).

Figure 5 illustrates the distribution of hardness from center to the edges of samples. As clear, the hardness distribution also has a similar trend with the nanoindentation and DSC results so that the hardness disposition is reversely correlated to the stored energy in the glassy structure. However, the detailed study of hardness shows that the rejuvenation process leads to intensified variations in the samples. In other words, the primary samples have a stable hardness distribution from the center to edges; however, a slight decrease is observed at the edges led by the faster cooling rate during the solidification. The faster cooling rate at the edges induces more free volume and disordered arrangement, which are the reason for hardness decrement. On the other side, there is no sign of increasing or decreasing trend in the hardness evolution, which means that the elastostatic loading significantly affects the whole atomic structure of samples and induce rejuvenation in the glassy material. However, the intensified variations of hardness in the different sites of sample, from center to edge, confirm the severe structural heterogeneity in HE-BMG alloys.

4 Conclusion

In this study, the effects of primary stored energy of HE-BMGs on the subsequent influence of elastostatic loading treatment were evaluated. According to the results, the minor addition of elements into the base alloying composition of HE-BMG, i.e., $Ti_{20}Zr_{20}Be_{20}Hf_{20}Cu_{20}$, led to the increase in the structural heterogeneity and stored energy. On the other side, an optimum primary stored energy was identified for obtaining maximum structural heterogeneity after the elastostatic loading. It was concluded that the rate of rejuvenation in HE-BMGs strongly depended on the free volume distribution and local elemental variations in the microstructure so that the low free volume distribution led to the increase in strength of backbone. Hence, an interstitial primary structural heterogeneity is needed for the

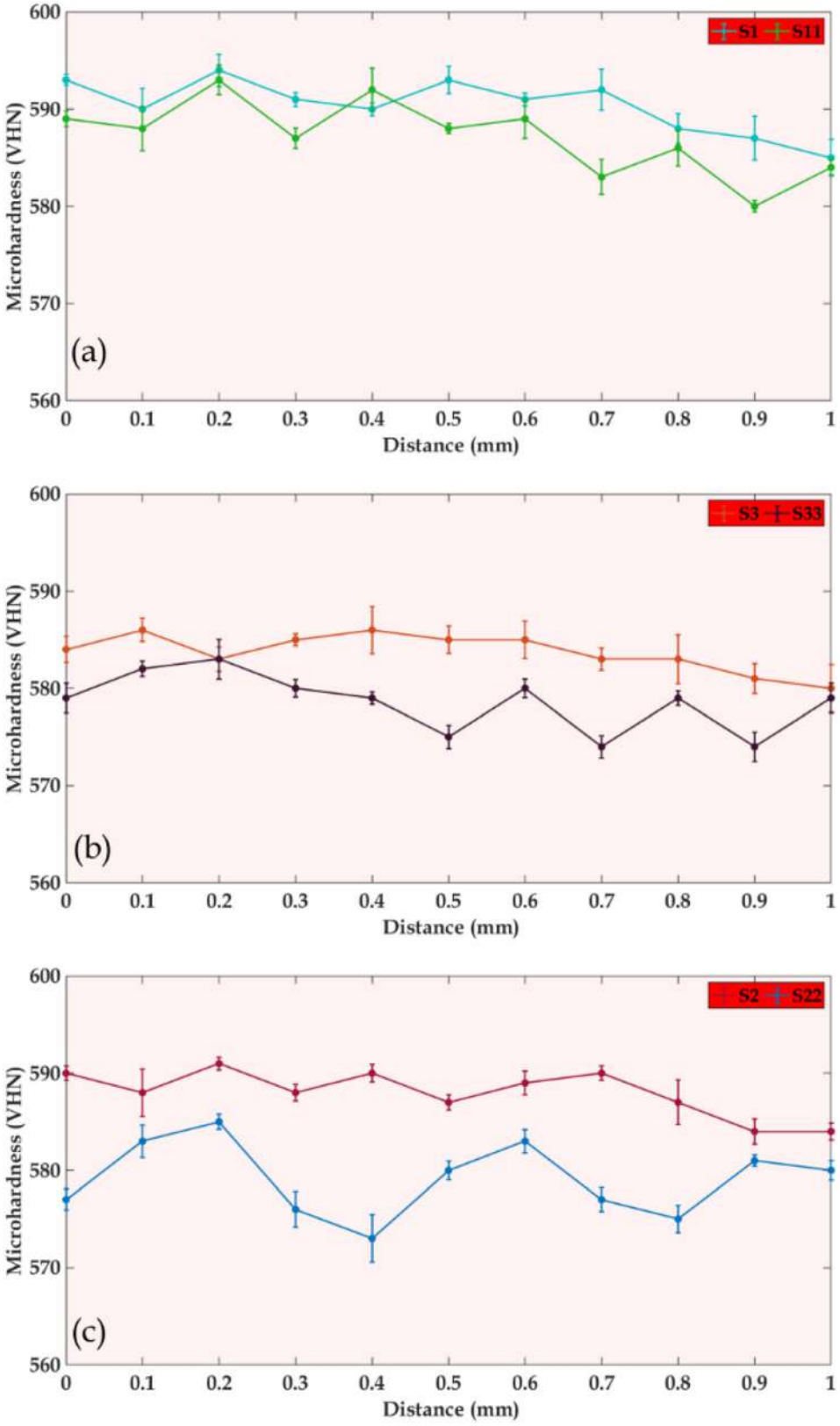

Fig. 5 Hardness distribution from center to edges for all the samples

maximum rejuvenation during elastostatic treatment in the HE-BMGs.

Acknowledgements The article was prepared as part of the state task "Research and development of complex energy-saving and thermo-electric regenerative systems" application number 2019-1497, subject number FZWG-2020-0034.

References

[1] Korkmaz S, and Kariper İ A, *J Non Cryst Solids* **527** (2020) 119753. https://doi.org/10.1016/j.jnoncrysol.2019.119753.
[2] Li Y, Shen Y, Leu M C, and Tsai H-L, *Mater Sci Eng A* **743** (2019) 404. https://doi.org/10.1016/j.msea.2018.11.056.
[3] Williams E, and Lavery N, *J Mater Process Technol* **247** (2017) 73. https://doi.org/10.1016/j.jmatprotec.2017.03.034.
[4] Bordeenithikasem P, Stolpe M, Elsen A, and Hofmann D C, *Addit Manuf* **21** (2018) 312. https://doi.org/10.1016/j.addma.2018.03.023.
[5] George E P, Curtin W A, and Tasan C C, *Acta Mater* **188** (2020) 435. https://doi.org/10.1016/j.actamat.2019.12.015.
[6] Ikeda Y, Grabowski B, and Körmann F, *Mater Charact* **147** (2019) 464. https://doi.org/10.1016/j.matchar.2018.06.019.
[7] Chen J, Zhou X, Wang W, Liu B, Lv Y, Yang W, Xu D, and Liu Y, *J Alloys Compd* **760** (2018) 15. https://doi.org/10.1016/j.jallcom.2018.05.067.
[8] Miracle D B, and Senkov O N, *Acta Mater* **122** (2017) 448. https://doi.org/10.1016/j.actamat.2016.08.081.
[9] Mollaqasem V K, Ardakani M H, and Hesaraki S, *J Res Sci Eng Technol* **1** (2013) 1.
[10] Wang W H, *JOM* **66** (2014) 2067. https://doi.org/10.1007/s11837-014-1002-3.
[11] Jin J, Li F, Yin G, Wang X, and Gong P, *Thermochim Acta* **690** (2020) 178650. https://doi.org/10.1016/j.tca.2020.178650.
[12] Qiao J, Pelletier J, Li N, and Yao Y, *J Iron Steel Res Int* **23** (2016) 19. https://doi.org/10.1016/S1006-706X(16)30005-X.
[13] Wu K, Liu C, Li Q, Huo J, Li M, Chang C, and Sun Y, *J Magn Magn Mater* **489** (2019) 165404. https://doi.org/10.1016/j.jmmm.2019.165404.
[14] Yang M, Liu X J, Ruan H H, Wu Y, Wang H, and Lu Z P, *J Appl Phys* **119** (2016) 245112. https://doi.org/10.1063/1.4955060.
[15] Li C, Li Q, Li M, Chang C, Li H, Dong Y, and Sun Y, *J Alloys Compd* **791** (2019) 947. https://doi.org/10.1016/j.jallcom.2019.03.375.
[16] Jiang W, and Zhang B, *J Appl Phys* **127** (2020) 115104. https://doi.org/10.1063/5.0002225.
[17] Glasscott M W, Pendergast A D, Goines S, Bishop A R, Hoang A T, Renault C, and Dick J E, *Nat Commun* **10** (2019) 2650. https://doi.org/10.1038/s41467-019-10303-z.
[18] Wang X, Dai W, Zhang M, Gong P, and Li N, *J Mater Sci Technol* **34** (2018) 2006. https://doi.org/10.1016/j.jmst.2018.04.006.
[19] Yin H, Huang Y, Daisenberg D, Xue P, Jiang S, Ru W, Jiang S, Bao Y, Bian X, Tong X, Shen H, and Sun J, *Scr Mater* **163** (2019) 29. https://doi.org/10.1016/j.scriptamat.2018.12.031.
[20] Huo J, Wang J-Q, Wang W-H, *J Alloys Compd* **776** (2019) 202. https://doi.org/10.1016/j.jallcom.2018.10.328.
[21] Wei R, Tao J, Sun H, Chen C, Sun G W, and Li F S, *Mater Lett* **197** (2017) 87. https://doi.org/10.1016/j.matlet.2017.03.159.
[22] Wang Y, Zhang K, Feng Y, Li Y, Tang W, Zhang Y, Wei B, and Hu Z, *J Nucl Mater* **527** (2019) 151785. https://doi.org/10.1016/j.jnucmat.2019.151785.
[23] Tong Y, Qiao J C, Pelletier J M, and Yao Y, *Intermetallics* **119** (2020) 106726. https://doi.org/10.1016/j.intermet.2020.106726.
[24] Wu J, Zhou Z, Yang H, Wang L, Liang X, Pi J, and Yi J, *J Alloys Compd* **827** (2020) 154298. https://doi.org/10.1016/j.jallcom.2020.154298.
[25] Gu J-L, Luan H-W, Zhao S-F, Bu H-T, Si J-J, Shao Y, Shao Y, and Yao, K-F, *Mater Sci Eng A* **786** (2020) 139417. https://doi.org/10.1016/j.msea.2020.139417.
[26] Duan YJ, Qiao JC, Crespo D, Goncharova E V, Makarov AS, Afonin G V, and Khonik V A, *J Alloys Compd* **830** (2020) 154564. https://doi.org/10.1016/j.jallcom.2020.154564.
[27] Samavatian M, Gholamipour R, Amadeh A A, and Mirdamadi S, *Mater Sci Eng A* 753 (2019) 218. https://doi.org/10.1016/j.msea.2019.03.058.
[28] Priezjev N V, *Comput Mater Sci* **168** (2019) 125. https://doi.org/10.1016/j.commatsci.2019.05.054.
[29] Das A, Dufresne E M, and Maaß R, *Acta Mater* **196** (2020) 723. https://doi.org/10.1016/j.actamat.2020.06.063.
[30] Samavatian M, Gholamipour R, Amadeh A A, and Mirdamadi S, *J Non Cryst Solids* **506** (2019) 39. https://doi.org/10.1016/j.jnoncrysol.2018.12.007.
[31] Wang T, Ma X, Chen Y, Qiao J, Xie L, and Li Q, *Intermetallics* **121** (2020) 106790. https://doi.org/10.1016/j.intermet.2020.106790.
[32] Wang Q, Zhou J, Zeng Q, Zhang G, Yin K, Liang T, Yang W, Stoica M, Sun L, and Shen B, *Materialia* **9** (2020) 100561. https://doi.org/10.1016/j.mtla.2019.100561.
[33] Samavatian M, Gholamipour R, Amadeh A A, and Samavatian V, *Phys B Condens Matter* **595** (2020) 412390. https://doi.org/10.1016/j.physb.2020.412390.
[34] Kosiba K, Şopu D, Scudino S, Zhang L, Bednarcik J, and Pauly S, *Int J Plast* **119** (2019) 156. https://doi.org/10.1016/j.ijplas.2019.03.007.
[35] Liu W-H, Sun B A, Gleiter H, Lan S, Tong Y, Wang X-L, Hahn H, Yang Y, Kai J-J, and Liu C T, *Nano Lett* **18** (2018) 4188. https://doi.org/10.1021/acs.nanolett.8b01007.
[36] Huo L S, Zeng J F, Wang W H, Liu C T, and Yang Y, *Acta Mater* **61** (2013) 4329. https://doi.org/10.1016/j.actamat.2013.04.004.